Astron. Astrophys. 343, 120–131 (1999)

ASTRONOMY AND ASTROPHYSICS

# Galactic dynamos driven by magnetic buoyancy

**David Moss**[1], **Anvar Shukurov**[2], **and Dmitry Sokoloff**[2,3]

[1] Department of Mathematics, University of Manchester, Manchester, M13 9PL, UK
[2] Department of Mathematics, University of Newcastle, Newcastle on Tyne, NE1 7RU, UK
[3] Physics Department, Moscow University, 19899 Moscow, Russia

Received 28 July 1998 / Accepted 13 November 1998

**Abstract.** We consider a mean field dynamo model for the generation of galactic magnetic fields, in which the driving mechanism for the alpha-effect is the buoyancy-driven Parker instability, rather than the conventional cyclonic turbulence. The dominant quenching mechanism is a buoyant velocity, which lifts field away from the disc plane. Our modified alpha-effect is essentially nonlinear, as its magnitude depends on the magnetic field strength. The dynamo thus exhibits threshold behaviour – the marginal dynamo number depends on the seed field geometry and strength. We investigate a basic one-dimensional 'slab' model both analytically and numerically, and also present results from a three dimensional calculation. In some ways our steady solutions resemble conventional galactic dynamo solutions, but the fields do not decrease so markedly away from the disc midplane, remaining strong out to the boundary of the dynamo region. The latter property is quite natural for a buoyancy driven system and may possibly be related to strong horizontal magnetic fields detected in the halos of some spiral galaxies.

**Key words:** galaxies: interactions – galaxies: magnetic fields – galaxies: ISM – ISM: magnetic fields – Magnetohydrodynamics (MHD) – magnetic fields

## 1. Introduction

Mean field dynamo models for the magnetic fields in spiral galaxies have been generically successful, in that they produce magnetic fields that resemble broadly those observed (e.g. Beck et al. 1996). A few attempts have been made to produce models tailored more specifically to individual galaxies, both in terms of kinematic dynamo models (Ruzmaikin et al. 1988 and references therein) and including alpha-quenching (Beck et al. 1996 and references therein). Although these models include only a few basic physical mechanisms and rely on a drastically simplistic description of the interstellar medium, they show a reassuring agreement between theory and observation (see, for example, a recent dynamo model for M31 in Moss et al. 1998). There have been several attempts to include additional physical effects into this framework. Among these are star formation (Ko & Parker 1989, Nozakura 1991), magnetic buoyancy (Parker 1992, Nozakura 1993, Hanasz & Lesch 1993, 1998 and references therein) and detailed models of turbulence (Elstner et al. 1996). Such work gives plausible evidence that the mean field theory provides a reasonable phenomenological description of galactic magnetic fields.

Nevertheless, doubts have been raised concerning the effectiveness of the basic alpha-effect mechanism. Vainshtein & Cattaneo (1992) and others have argued that the alpha-effect will be inhibited by the growth of small-scale field long before the large-scale field can grow to the observed microgauss strength. Although this viewpoint is not firmly established or universally accepted (see, e.g., Brandenburg 1994, Childress & Gilbert 1995, Beck et al. 1996), the situation is perhaps a little unsatisfactory. In contrast, the rôle of differential rotation in galaxies appears relatively uncontroversial (unlike the situation for stars), given that the transparency of galaxies allows direct, if technically difficult, determination of rotation curves.

Parker (1992) suggested an alternative mechanism to perform the conversion of the toroidal into poloidal field in the dynamo process, a step for which the alpha-effect is responsible in conventional mean-field dynamos. He observed that strong magnetic field parallel to the disc plane will be subject to a buoyant instability (the 'Parker instability'). This causes the field to buckle and rise in $\Omega$-shaped loops inflated by cosmic rays, which in form resemble those in the cartoons of the original alpha-effect (see e.g. Moffatt 1978). A mean-field theory incorporating this mechanism would resemble quite closely the traditional theory, with two major differences. The buoyant alpha mechanism leads to an intrinsically nonlinear equation, with the magnitude of the alpha effect increasing with field strength (Moffatt 1978, Sect. 10.7), and it would not be inhibited at low amplitude of the large scale field, following arguments of the sort proposed by Vainshtein & Cattaneo (1992).

Intrinsically nonlinear dynamos driven by magnetostrophic waves and by buoyancy and nonaxisymmetric instabilities of flux tubes were studied by Schmitt (1987), Schmitt & Schüssler (1989), Schüssler (1993), Ferriz-Mas et al. (1994) in applications to the solar dynamo. These authors show that the instabilities lead to an alpha-effect, and then analyze conventional mean-field equations, including magnetic buoyancy only to describe the escape of magnetic fields from the dynamo region at

*Send offprint requests to*: D. Moss

a velocity proportional to the mean field strength $|\boldsymbol{B}|$. Nonlinear saturation of conventional mean-field dynamos by magnetic buoyancy was also extensively studied in the numerical simulations of Moss et al. (1990a,b) and Jennings & Weiss (1991). In the context of stellar dynamos, Thelen (1997) has included a buoyant alpha-effect proportional to the gradient of toroidal field strength, but disregarded the buoyant rise of the mean field. Brandenburg et al. (1998) included both a field-dependent alpha-effect and explicit magnetic buoyancy into their model of stellar mean-field dynamos.

An alpha-effect based on magnetic buoyancy was discussed for a disc geometry in a series of papers by Hanasz & Lesch (1998 and references therein), but these authors did not discuss in detail its dependence on the magnetic field strength nor present any quantitative model of the dynamo itself.

We investigate the properties of a buoyant alpha-effect dynamo, in a heuristic manner, taking its magnitude to be a function of the field strength or its gradient. Of course, by itself this would lead to an unlimited explosive (super-exponential) field growth. But the same buoyancy will lift field away from the disc plane into the halo region, and damp the dynamo. We thus introduce a buoyant velocity, perpendicular to the disc plane, with magnitude a fraction of the Alfvén speed, and so proportional to the field strength. In Sect. 2 we argue that this is the dominant saturation mechanism over a wide range of parameters. A novel, albeit not unexpected, feature of such a dynamo is that it will display threshold behaviour – because the magnitude of the effective alpha-coefficient is itself proportional to the field strength, excitation will only occur if the seed field, for given dynamo number, exceeds some critical value. The relatively strong seed field for the buoyant dynamo may be provided by a conventional alpha-effect dynamo; in this sense, the rôle of the conventional alpha-effect is trivial, and we do not include it in our equations.

We reduce the complexity of the Parker instability to a description in terms of just two parameters, $u_B$ and $\alpha$ (see Sect. 2). We do not discuss in detail the physical mechanisms driving the instability. Therefore questions such as the contribution of the cosmic rays to the buoyancy (Parker 1992, Hanasz & Lesch 1998) are beyond the scope of the paper. Furthermore, we do not address such issues as the dependence of the Parker instability threshold on the field strength and scale.

## 2. The alpha effect due to magnetic buoyancy

In this section we first derive an order of magnitude estimate of the mean helicity of the buoyancy driven motions in the interstellar medium and hence estimate the associated alpha-coefficient. As with the standard alpha-effect, the mirror symmetry of the motions is broken due to the action of the Coriolis force in the stratified medium (Parker 1979, Krause & Rädler 1980). A buoyant rising fluid element expands because it is inflated by cosmic rays, so it is twisted by the Coriolis force (Parker 1992). However, twisting also results from the local motion present as the gas slides down a buckled flux tube. We estimate the alpha-coefficient for each of these mechanisms below.

Consider a magnetic flux tube moving vertically upwards in the galactic disc. Its vertical velocity is given by

$$u_B = C\,(d/z_0)^{1/2}\,v_A\ ,$$

where $d$ is its radius, $z_0$ is the pressure scale height, $v_A$ is the Alfvén speed and $C$ is a constant of order unity; with $d \simeq z_0$, we have $u_B \simeq v_A$ (e.g., Parker 1979, Sect. 8.7). The rising fluid element expands as a result of inflation by cosmic rays (Parker 1992), and the fluid acquires a horizontal velocity $v_r$ given by the continuity equation $\nabla \cdot (\rho \boldsymbol{v}) = 0$ as $v_r \simeq u_B l/z_0$, where $l$ is its size (we use a local cylindrical coordinate system centred at the fluid element). The Coriolis force twists the fluid element producing an acceleration $\boldsymbol{a} = 2\boldsymbol{\Omega} \times \boldsymbol{v}$ which results in the generation of vorticity directed oppositely to the overall angular velocity $\boldsymbol{\Omega}$: $\omega_z \simeq \tau \partial a_\phi/\partial r \simeq -\tau\Omega v_r/l \simeq -\Omega$, where $\tau \simeq z_0/u_B$ is the characteristic time of the problem; alternatively, $\omega_z = -\Omega$ can be directly obtained from the conservation of angular momentum. However, the magnitude of the vorticity is limited from above by the value $|\omega_z| \simeq v_A/l$. As a result, the magnitude of the vorticity is the minimum of the above two values, or $\omega_z = \max(-\Omega, -v_A/l)$. The associated alpha-coefficient is given by

$$\alpha \simeq -\tau u_B \omega_z \simeq \min(z_0\Omega, v_A z_0/l)\ . \qquad (1)$$

Another mechanism to produce the alpha-effect from magnetic buoyancy does not involve cosmic rays. When a magnetic flux tube rises, the gas acquires a radial velocity because it slides down under the action of gravity. When the free-fall time $\tau_{\rm ff} = (z_0/g)^{1/2}$ (here $g$ is the acceleration due to gravity) is shorter than the buoyancy time $z_0/u_B$, the gas can reach the bottom of the rising $\Omega$-shaped loop. Then $v_r \simeq l/\tau_{\rm ff}$, where $l$ is the horizontal scale of the Parker instability, and $\omega_z \simeq -\Omega$ as above. The upper limit on $\alpha$ follows from $|\omega_z| \lesssim v_A/l$ and $u_B \lesssim v_{\rm ff} = (g z_0)^{1/2}$, so that

$$\alpha \simeq -\tau_{\rm ff} u_B \omega_z \simeq \min\left(C v_A \Omega (d/g)^{1/2}, v_A z_0/l\right)\ . \qquad (2)$$

To put these estimates into appropriate perspective, we recall that a similar estimate for the standard alpha-coefficient for turbulence in a stratified rotating medium is given by $\alpha = \min(l^2\Omega/z_0, v_t)$, where $v_t$ is the turbulent velocity (Zeldovich et al. 1983; Ruzmaikin et al. 1988, p. 163).

For a relatively weak magnetic field the alpha-coefficient is proportional to the Alfvén speed within a magnetic flux tube. As the magnetic field grows due to the dynamo action, the alpha-coefficient also increases (with ensuing super-exponential growth of the magnetic field, in the absence of any damping). Saturation effects, for example associated with the lifting of the magnetic field by the vertical velocity $u_B$, eventually will halt the field growth. These processes are well illustrated by our dynamo solutions discussed below.

A further effect that may eventually inhibit dynamo action is the effect of magnetic tension, in resisting the rotation of the $\Omega$-shaped loops by the Coriolis force (i.e. a form of 'alpha-quenching'). We can make a crude estimate of the importance of this effect as follows. Consider a horizontal field $B_0$ in the

azimuthal direction, in a gas that undergoes Parker instability with wavelength $l$. Suppose that the buckled loop is rotated by the Coriolis force at speed $v_\phi$ during time $\tau$. Take a local cartesian system of coordinates, so that $B_x = B_0$. Then at time $\tau$, $B_y = -B_0 v_\phi \tau / l \sin(\pi x/l)$. The Lorentz force is thus

$$\left| \frac{\nabla \times \mathbf{B} \times \mathbf{B}}{4\pi} \right| \sim \frac{B_0^2 v_\phi \tau}{4l^2} = L, \tag{3}$$

say. With $v = \Omega l$ as above, then $L = B_0^2 \Omega \tau/(4l)$. This opposes the component $2\rho\Omega v_r$ of the Coriolis force.

We consider separately the two cases identified above.
1. $\tau = z_0/u_B$, $v_r = u_B l/z_0$. Then

$$L = \frac{B_0^2 z_0 \Omega}{4 l u_B}. \tag{4}$$

Saturation does not occur as long as

$$L < 2\rho\Omega u_B l/z_0. \tag{5}$$

$B_0$ drops out of this relation and thus, if the Parker instability is launched, in this case it is never halted by the magnetic tension.
2. $\tau = (z_0/g)^{1/2}$, $v_r = l/\tau_{\rm ff} \simeq l\sqrt{g/z_0}$. Now saturation does not occur as long as

$$L = \frac{B_0^2 \Omega}{4l} \left( \frac{z_0}{g} \right)^{\frac{1}{2}} < 2\rho\Omega l \left( \frac{g}{z_0} \right)^{\frac{1}{2}}, \tag{6}$$

ie $B_0^2 < 8\rho g l^2/z_0$. Defining $B_{\rm eq}^2 = 4\pi\rho v_t^2$, and inserting as typical values $v_t = 10^6\,{\rm cm\,s^{-1}}$, $g = 6 \times 10^{-9}\,{\rm cm^2\,s^{-1}}$, $l = 1\,{\rm kpc}$, $z_0 = 0.5\,{\rm kpc}$, gives $B_0 \lesssim 5 B_{\rm eq}$. Thus alpha-quenching is only effective for large-scale fields of strength considerably in excss of the equipartition field strength.

Referring ahead to our numerical results, we see that this mechanism is important only when $R_b = 1$, or for very supercritical solutions.

To conclude this section, we estimate typical values of $\alpha$ in the interstellar medium of the Milky Way. For $\Omega = 20\,{\rm km\,s^{-1}\,kpc^{-1}}$, $z_0 = 1\,{\rm kpc}$, $g \simeq 6 \times 10^{-9}\,{\rm cm\,s^{-2}}$ (at a height of $1\,{\rm kpc}$), $v_A = 20\,{\rm km\,s^{-1}}$ (corresponding to magnetic field of $3\,\mu{\rm G}$ and density of $0.1\,{\rm cm^{-3}}$ in the flux tube), $d = z_0$ and $l = k z_0$ with $k$ ($\geq 1$) a certain constant, we obtain from Eq. (1) $\alpha = \min(20, 20k^{-1})\,{\rm km\,s^{-1}}$, so a suitable estimate is $\alpha \simeq v_A z_0/l$ provided $k \gtrsim 1$. Eq. (2) yields similar values, $\alpha = \min(15C, 20k^{-1})\,{\rm km\,s^{-1}}$. The resulting value of $\alpha$ is close to $v_A$ in both cases; however, we have persistently omitted numerical coefficients of order unity, so real values of $\alpha$ can be a few times smaller than $v_A$.

## 3. The basic model

We start from a standard mean-field dynamo equation

$$\frac{\partial \boldsymbol{B}}{\partial t} = \nabla \times (\boldsymbol{u} \times \boldsymbol{B} + \alpha \boldsymbol{B} - \eta \nabla \times \boldsymbol{B}) \ , \tag{7}$$

where $\eta$ is the turbulent magnetic diffusivity and the large-scale velocity $\boldsymbol{u}$ is taken to consist of the rotational velocity $r\Omega(r)\hat{\boldsymbol{\phi}}$, and a vertical velocity $u_B(z)\hat{\boldsymbol{z}}$. We use cylindrical polar coordinates ($r$, $\phi$, $z$), with the $z$-axis parallel to the angular velocity. The form of this equation is quite generic and can be obtained from simple symmetry considerations (Krause & Rädler 1980). Particular dynamo models differ in the specific parameterization of the coefficients in this equation reflecting different physical mechanisms responsible for the diffusion and generation of the mean magnetic field.

We concentrate here on the dynamo effect associated with magnetic buoyancy when $\alpha$ and $u_B$ are both proportional to $v_A$ (Sect. 2) with the additional restriction that they must be antisymmetric with respect to the midplane. Thus, we choose

$$\alpha = \alpha_0 f_\alpha(\boldsymbol{r}) F(\boldsymbol{B}/B_{\rm eq}) \ , \tag{8}$$

$$u_B = q v_t f_b(\boldsymbol{r}) F(\boldsymbol{B}/B_{\rm eq}) \ , \tag{9}$$

where $F(\boldsymbol{B}/B_{\rm eq})$ is a function of the dimensionless magnetic field, $B_{\rm eq} = (\mu_0 \rho v_t^2)^{1/2}$ is the characteristic field strength determined by a balance of magnetic and turbulent pressures, $\rho$ and $v_t$ are respectively the density and r.m.s. velocity of the turbulent interstellar medium, $\alpha_0$ has the dimension of velocity, $q$ is a numerical factor defining the magnitude of the buoyant velocity, and $f_\alpha(\boldsymbol{r})$ and $f_b(\boldsymbol{r})$ are geometric factors, of order unity; the factors $\alpha_0$ and $q$ include the filling factor of the buoyant magnetic ropes. In principle, $F$ could depend on the horizontal field strength $(B_r^2 + B_\phi^2)^{1/2}$. We consider briefly such a model in Sect. 4.5. The results are very similar to those for $F = |B_\phi|/B_{\rm eq}$. As the latter form allows an analytic treatment, we use it as a basic model. We henceforth drop the subscript on the azimuthal component of the magnetic field, i.e. $B_\phi \equiv B$.

The forms (8) and (9) arise when the buoyant magnetic field is concentrated into flux tubes (Schmitt & Schüssler 1989): then $u_B$ is proportional to the difference between the field strength inside the tube and in its environment. For a quasi-homogeneous distribution of the buoyant magnetic field, $u_B$ is determined by the vertical gradient of the field strength; then $\alpha, u_B \propto -\partial|B|/\partial z$ may be more appropriate (cf. Thelen 1997, who however did not include the term $u_B$). We briefly discuss the latter form below.

Another component of the vertical velocity is associated with turbulent diamagnetism, $\boldsymbol{u}_{\rm dia} = -\frac{1}{2}\nabla\eta$ (Rädler 1968, Vainshtein & Zeldovich 1972, Roberts & Soward 1975). It is included in the three-dimensional models discussed below.

We consider here only crude, exploratory models of buoyancy driven dynamos. Therefore our parameterization of $\alpha$ and $u_B$ satisfies only a few basic requirements – that both of them vanish at $z = 0$ and that $f_b \propto z^n, n \geq 1$ for $z \approx 0$ in order that $u_B$ be differentiable at $z = 0$; we choose $n = 1$ for reasons discussed in Sect. 4.1. For large $z$, we adopt $f_b = 1$, although $f_b$ could well be a decreasing function of $z$.

The parameterization of the buoyancy as a large-scale vertical velocity is quite natural in the context of a mean field representation – see, for example, Krause & Rädler (1980), Rädler (1990). However, we realize that buoyancy has also been considered as a contribution to the diffusivity. Nevertheless, we neglect any contribution of the vertical motions to the turbulent magnetic diffusivity. A plausible model might make $\eta$ proportional

to $v_A$ (Hanasz & Lesch 1998). Then magnetic diffusion would be stronger where the field is stronger. However, the steady-state field distributions discussed below do not depend strongly on $z$, so the functional dependence of $\eta$ on $\boldsymbol{B}$ is expected to be relatively unimportant.

The governing parameters of the model are the dimensionless numbers

$$R_\alpha = \frac{\alpha_0 h}{\eta} \ , \quad R_\omega = r\frac{d\Omega}{dr}\frac{h^2}{\eta} \ , \quad R_b = \frac{q v_t h}{\eta} \ ,$$

where $h$ is a suitable length scale. In the $\alpha\omega$-dynamo regime, the first two of these combine to give the dynamo number

$$D = R_\alpha R_\omega \ .$$

Almost certainly the contribution of the magnetic buoyancy to the diffusivity is now an anisotropic tensor; its $zz$-component, which is most important in a thin disc, can be estimated as $\eta \simeq \frac{1}{3} l v_A \simeq 2\times 10^{27}\,\mathrm{cm^2\,s^{-1}}$, where $l \simeq 1\,\mathrm{kpc}$ is the scale from the Parker instability. Using estimates of Sect. 2 with $h = z_0$, we then obtain $R_\alpha \simeq R_\omega \simeq 3$ and $R_b \simeq 3qh/l \simeq 3q$; we present results for $1 \le R_b \le 10$.

The large value of $l \simeq 1\,\mathrm{kpc}$ associated with the Parker instability makes the ratio $R_\alpha/R_\omega$ larger than for conventional dynamos. Therefore, we can expect $\alpha^2$-dynamo effects to be more pronounced in buoyancy-driven dynamos than in conventional ones. This may facilitate the generation of nonaxisymmetric and dipole fields. On the other hand, the larger vertical extent of the dynamo active region will act to suppress nonaxisymmetric fields, so the existence and persistence of nonaxisymmetric solutions will depend on details of the model.

The fundamental difference between dynamos based on magnetic buoyancy and conventional dynamos is that the former are intrinsically nonlinear and, apart from sufficiently large $R_\alpha$ and/or $R_\omega$, they require a sufficiently strong initial fields for the dynamo instability to occur. This field can be provided *ab initio* or generated by a conventional dynamo. We anticipate that the regimes of weak and strong initial field have distinct excitation conditions. Some aspects of this issue are explored in Sect. 4.4.

We consider two types of models. In Sect. 4 we describe and investigate a local slab model, in the spirit of that described by, e.g., Ruzmaikin et al. (1988). In Sect. 5 we examine a three-dimensional dynamo model.

## 4. A local analysis

The standard local slab approximation (see, e.g., Ruzmaikin et al. 1988, Sect. VII.5), removes the explicit radial dependence from the problem by assuming $\partial/\partial r = 0$ everywhere, except in the dependence of $\Omega$ on $r$. We further consider axisymmetric solutions, so $B_r = -\partial A/\partial z$ and $B_z = r^{-1}\partial(rA)/\partial r$, with $A$ the $\phi$-component of the vector potential, and we continue to denote $B_\phi = B$. Eq. (7) is now nondimensionalized in terms of a characteristic length $h$, and a time $h^2/\eta$, and we write $\widetilde{B} = B/B_{\rm eq}$, $\widetilde{A} = A/(R_\alpha h B_{\rm eq})$. Using expressions (8) and (9), and dropping the tildes on the dimensionless quantities, this results in

$$\frac{\partial A}{\partial t} = f_\alpha |B| B - R_b \frac{\partial A}{\partial z}|B| f_b + \frac{\partial^2 A}{\partial z^2} \ , \tag{10}$$

$$\frac{\partial B}{\partial t} = -D\frac{\partial A}{\partial z} - R_b \frac{\partial}{\partial z}(|B| B f_b) + \frac{\partial^2 B}{\partial z^2} \ . \tag{11}$$

The standard treatment takes $h$ to be the slab semi-thickness. We generalize this slightly, in that we take $f_\alpha = \sin(\pi z/z_\alpha)$ in $0 \le z \le z_\alpha$, and zero elsewhere, thus confining the alpha effect to the region $0 \le z \le z_\alpha$ in order to investigate the rôle of a dynamo passive layer in Sect. 4.3. We take $f_b = z/z_b$ for $z \le z_b$, and $f_b = 1$ for $z_b < z \le 1$, where we put $z_b = z_\alpha/2$. When $z_\alpha < 1$, the effective dynamo number, based on the size of the dynamo-active region, is $\mathcal{D} = z_\alpha^2 D$. With this definition, the critical (i.e. marginal for excitation) value of $\mathcal{D}$ tends to a finite value as $z_\alpha \to 0$ (see Fig. 3b).

We are mostly interested in fields of even parity, for which the appropriate boundary condition on $z = 0$ is $A = \partial B/\partial z = 0$. (We find that even parity fields are much more readily excited than odd, as in conventional $\alpha^2\omega$-dynamos – Sect. 4.5). The usual vacuum-like boundary condition on $z = 1$ is $B = \partial A/\partial z = 0$. However the condition $B = 0$ on $z = 1$ may be inappropriate to the physical situation discussed here, where field is being advected away from the disc and out of the slab, and an alternative condition, such as $\partial B/\partial z = 0$ on $z = 1$, might be more suitable. In fact, the only effect of setting $B = 0$ on $z = 1$ in this slab model is to generate a boundary layer in which $B \to 0$, near $z = 1$. This boundary layer steepens as $|D|$ increases. Outside of the boundary layer, the solution is almost indistinguishable from that found with the boundary condition $\partial B/\partial z = 0$. The value of $|D|$ at which excitation first occurs is slightly larger when the condition $B = 0$ is used on $z = 1$.

Eqs. (10) and (11) follow from (7), with $u_B, \alpha \propto |B|$. If we take $u_B, \alpha \propto -\partial|B|/\partial z$, when $\partial|B|/\partial z < 0$ and 0 otherwise (cf. Thelen 1997), then $|B|$ must be replaced by $-\partial|B|/\partial z$ in Eqs. (10) and (11), and we may take $f_\alpha = f_b = 1$. We were unable to find any physically nontrivial solutions in this case. An exact steady solution of the equations is $B =$ constant and $A =$ constant. With the boundary condition $B = 0$ at $z = 1$, this solution is trivial. For $\partial B/\partial z = 0$ at $z = 1$, this solution has $B_r = 0$ and $B$ an arbitrary constant. Although we cannot prove that this solution is unique, modest numerical experimentation did not find any non-trivial solutions. With $u_B \propto |B|$, $\alpha \propto -\partial|B|/\partial z$, we found only steady solutions with such field distributions when $\alpha$ differs significantly from zero only in a boundary layer near $z = 1$. Such solutions appear physically uncompelling and we do not consider them further. Note that these analytical arguments do not exclude oscillatory solutions with such a choice of $\alpha$ and $u_B$. However, as noted, such solutions were not found during the numerical experimentation.

### 4.1. An approximate solution

Before discussing numerical solutions of Eqs. (10) and (11), we present their approximate steady state solution for $|D| \gg 1$. In

the steady state, Eqs. (10) and (11) reduce to

$$B''' - R_b(f_bB^2)'' - R_bf_bBB'' + R_b^2f_bB(f_bB^2)' + Df_\alpha B^2 = 0 \,, \quad (12)$$

$$B_r = -D^{-1}B'' + R_bD^{-1}(f_bB^2)' \,, \quad (13)$$

where prime denotes differentiation with respect to $z$. We consider $B(0) > 0$ here; the case $B(0) < 0$ will be discussed separately.

The steady state is described by a third-order, rather than fourth-order, equation. This is true also for conventional $\alpha\omega$-dynamos. One of the four boundary conditions, $A(0) = 0$, is a consequence of the relations $B'(0) = 0$, $f_\alpha(0) = 0$ and the steady-state governing equation, so we are left with three independent boundary conditions (Kvasz et al. 1992).

It can be expected that $|B| \gg 1$ when $|D| \gg 1$. Assuming that there are no boundary layers (so $B' = \mathrm{O}(B)$), the orders of magnitude of the consecutive terms in Eq. (12) are $B, B^2, B^2, B^3$ and $DB^2$, respectively. Retaining terms with the highest powers of $D$ and $B$, we obtain the following lowest-order equation:

$$R_b^2f_bB(f_bB^2)' + Df_\alpha B^2 = 0 \quad (14)$$

for $D \gg 1$. The physical meaning of this approximate solution is that the steady state is established when buoyant rise of magnetic field from the dynamo active region $|z| \le z_\alpha$ (the first term) balances the dynamo action (the second term), whereas magnetic diffusion ($B'''$) is less important. Eq. (14) can be easily solved in terms of the dependent variable $f_bB^2$ to yield the following solution finite at $z = 0$:

$$B = -\frac{D}{2R_b^2}f_b^{-1/2}\int_0^z \frac{f_\alpha}{f_b^{3/2}}\,dz' \,, \quad (15)$$

and the corresponding leading term in the asymptotic expansion for $B_r$ is

$$B_r = \frac{R_b}{D}(f_bB^2)' = -\frac{1}{R_b}\frac{f_\alpha}{f_b}B \,. \quad (16)$$

We note that if $f_\alpha \propto z$, then Eq. (15) yields an even-parity solution without a boundary layer at $z = 0$ only when $f_b \propto z$ as $z \to 0$. More generally, $B \sim z^{1+m-2n}$ for $f_b \propto z^n$ and $f_\alpha \propto z^m$. Thus, $B(0) = 0$ for $n < (1+m)/2$ and $B(0) \to \infty$ for $n > (1+m)/2$. Hence, the choice $f_\alpha, f_b \propto z$ for $z \ll 1$ is unique if there is to be no boundary layer at $z = 0$ and if $f_\alpha$ and $f_b$ behave similarly at $z \approx 0$, i.e., $n = m$.

With $f_b, f_\alpha \propto z$ for $z \to 0$, the solution (15), (16) fortuitously satisfies all boundary conditions, $B'(0) = A'(1) = B'(1) = 0$.

For $z > z_\alpha, z_b$, Eqs. (15) and (16) yield $B =$ constant and $B_r = 0$. It can be shown that this is an exact solution of the complete Eqs. (12) and (13) with the boundary condition $B'(1) = 0$ for those values of $z$ where $f_\alpha = 0$ and $f_b = 1$. Indeed, consider a neighbourhood of $z = 1$: then $B' \approx 0$ from the boundary condition, $B'' \approx 0$ from Eq. (13) since $B_r(1) \equiv -A'(1) = 0$, and then $B''' = 0$ due to Eq. (12). Since all the derivatives entering Eq. (12) vanish at $z = 1$, $B =$ constant is the unique solution; this can be easily proved using the Cauchy-Euler approximation method for the proof of the existence theorem for ordinary differential equations (see e.g. Hurewicz, 1958). Our numerical solutions show that the boundary condition $B(1) = 0$ results in a boundary layer near $z = 1$ as $|D|$ increases but the solution remains close to that for $B'(1) = 0$ outside the boundary layer.

It can be easily verified that both $(A, B)$ given by Eqs. (15), (16) and the corresponding $(-A, -B)$ are solutions of Eq. (12) for $D < 0$ if $f_\alpha > 0$ at $z > 0$. For $D > 0$ there are no nontrivial solutions since the signs of $B$ and $D$ in a relation similar to Eq. (15) do not match for $f_\alpha > 0$. For $f_\alpha < 0$, nontrivial solutions exist only for $D > 0$. Explicit expressions for the solution are given in Appendix A.

Substituting the asymptotic solution (15), (16) into Eq. (12) and comparing the terms included in Eq. (14) with those neglected, we obtain $D \gg R_b$ as the condition for the validity of the asymptotic solution. The solution may be inapplicable for very small $z_\alpha$ because the terms $B'' \propto z_\alpha^{-1}$ and $B''' \propto z_\alpha^{-2}$ are no longer negligible.

In the following sections we discuss numerical solutions of the initial-boundary value problem for Eqs. (10) and (11) for both $z_\alpha = 1$ (a slab surrounded by vacuum) and $z_\alpha < 1$ (a dynamo active slab within a layer in which the alpha-effect vanishes).

### *4.2. Slab surrounded by vacuum*

We first took the simplest model, putting $z_\alpha = 1$, $z_b = 0.5$, imposing as initial condition an arbitrary seed field given by

$$B(z) = \sin\pi z \,, \quad A(z) = z(1-z) \,. \quad (17)$$

We chose a 'standard' value of $R_b = 1$, and varied $D$. We solved Eqs. (10) and (11) by a simple time-stepping method, and found that the field evolved to a steady configuration when $D < D_{\rm cr} \approx -(13.0\text{–}13.5)$. Steady solutions were found for larger values of $|D|$, although an increasingly fine spatial grid and small time step were needed as $|D|$ became large. The critical value of the dynamo number is $D_{\rm cr} \approx -8$ for the analogous problem with a conventional alpha-effect – see e.g. Ruzmaikin et al. (1988, Sect. VII.5). It is reassuring that the excitation conditions for the mean-field disc dynamo change so little when different physical mechanisms leading to the alpha-effect are chosen.

Results are summarized in Table 1, and the dimensionless field components $B(z)$ and $B_r(z)$ are plotted in Fig. 1 for the case $D = -15$. Note that transformation to physical units requires that $B$ is multiplied by $B_{\rm eq}$, whereas $B_r$ must be multiplied by $R_\alpha B_{\rm eq}$. Thus the ratio $B_r/B_\phi$ in physical units depends, for a given value of $D$, on the relative importance of the alpha-term and the shear from the differential rotation. Larger values of $R_b$, corresponding to increased advection of field away from the disc plane, not unexpectedly make the dynamo harder to excite – see Table 1. In Fig. 1 we also show the approximate solution (with the boundary condition $\partial B/\partial z = 0$ at $z = 1$). There is a fair agreement between the approximate and numerical solutions, even for this relatively low value of $D = -15$. For

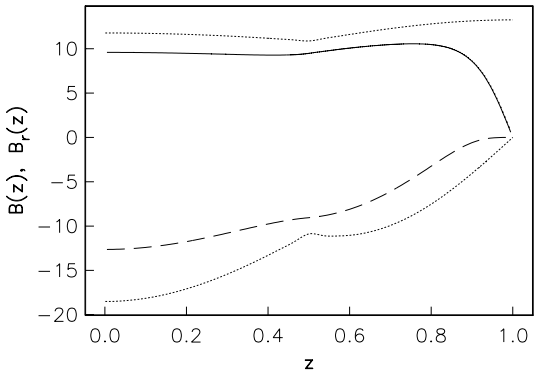


**Fig. 1.** The steady-state solutions of Eqs. (10) and (11) for the dimensionless azimuthal and radial field components, $B$ (solid) and $B_r$ (broken). The corresponding approximate solutions, Eqs. (15) and (16), are shown with dotted lines. Here $z_\alpha = 2z_b = 1$, $R_b = 1$ and $D = -15$.

**Table 1.** Steady-state solutions of Eqs. (10) and (11) for $z_\alpha = 2z_b = 1$ and the seed field given by (17). The values of the dimensionless azimuthal and radial field components, $B$ and $B_r$, are given at the slab midplane $z = 0$ for various values of the dynamo number $D$ and the buoyancy number $R_b$. These dimensionless values transform to physical field strengths as specified in Sect. 4.

| $D$ | $B(0)$ | $B_r(0)$ |
|---|---|---|
| $R_b = 1$ | | |
| $-13$ | decays | |
| $-13.5$ | 8.5 | $-11.0$ |
| $-14$ | 8.8 | $-11.5$ |
| $-15$ | 9.6 | $-12.6$ |
| $-20$ | 13.4 | $-18.3$ |
| $-50$ | 36.9 | $-54.9$ |
| $-100$ | 76.2 | $-117.0$ |
| $R_b = 5$ | | |
| $-40$ | decays | |
| $-41$ | 0.75 | $-0.15$ |
| $-42$ | 0.8 | $-0.17$ |
| $-50$ | 1.2 | $-0.27$ |
| $-100$ | 2.7 | $-0.73$ |
| $-200$ | 5.8 | $-1.70$ |
| $R_b = 10$ | | |
| $-80$ | decays | |
| $-82$ | 0.37 | $-0.04$ |
| $-85$ | 0.42 | $-0.05$ |
| $-100$ | 0.57 | $-0.07$ |
| $-200$ | 1.34 | $-0.18$ |
| $-500$ | 3.69 | $-0.55$ |

larger values of $|D|$, where the approximate solution is strictly applicable, the agreement is remarkably good (see also Fig. 3c).

We noticed that this model does display threshold behaviour, in that if $D$ is fixed at a supercritical value, then excitation only occurs if the strength of the seed field exceeds a certain value. We discuss this phenomenon in more detail in Sect. 4.4.

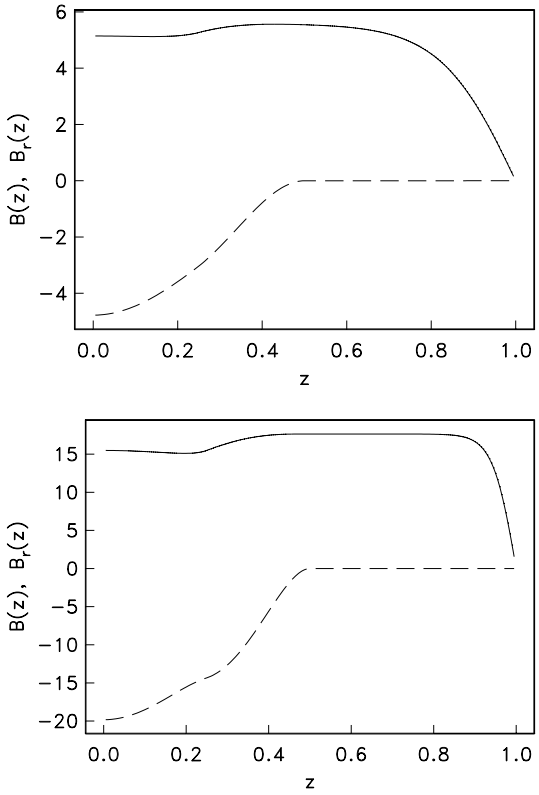


**Fig. 2.** Dimensionless field components $B(z)$ (solid) and $B_r(z)$ (broken) for the one-dimensional model with $z_\alpha = 2z_b = 0.5$ and $R_b = 1$. *Upper panel:* $D = -23$ (marginally supercritical solution); *lower panel:* $D = -50$ (strongly supercritical solution).

### *4.3. Slab surrounded by a passive halo*

We next discuss models that simulate the presence of a passive halo by taking $z_\alpha < 1$. We again used the seed field (17) in all the calculations reported in this section. We summarize results from calculations with $z_\alpha = 0.5, 0.3$ and 0.2 in Table 2, with $1 \le R_b \le 10$. The dimensionless field components $B(z)$ and $B_r(z)$ for the marginally and substantially supercritical cases $D = -23$ and $-50$ at $R_b = 1$, $z_\alpha = 0.5$, are plotted in Fig. 2.

Comparison of the two panels of Fig. 2 shows clearly the development of the boundary layer near $z = 1$ as $|D|$ increases. A notable feature of our results is that the radial field $B_r$ is confined to the region $|z| \lesssim z_\alpha$; this can be also seen from Eq. (16). We illustrate in Fig. 3 how the system responds to variations in $R_b$ and $z_\alpha$. The spatial distributions of $B$ and $B_r$ do not change much as $D$ and $z_\alpha$ vary, but the field strength increases as $|D|$ increases or $z_\alpha$ decreases, as $B(0) \propto z_\alpha^{-1}, B_r(0) \propto z_\alpha^{-1}$, at fixed $\mathcal{D}$ ($= z_\alpha^2 D$) and $R_b$ with $z_b = \frac{1}{2} z_\alpha$, in remarkable agreement with the approximate solution of Sect. 4.1 and Appendix A (note that $D$, and not $\mathcal{D}$, appears in this Appendix).

$|\mathcal{D}_{\rm cr}|$ increases linearly with $R_b$ (Fig. 3a), and the slope increases as $z_\alpha$ decreases. When $R_b = 1$, $|\mathcal{D}_{\rm cr}|$ decreases monotonically as $z_\alpha$ decreases at fixed $R_b$, and reaches the value $\mathcal{D}_{\rm cr} \approx -3.5$(Fig. 3b); it is surprising that Eq. (B2) gives an estimate $\mathcal{D}_{\rm cr} \simeq -4$ that is so close to this value. The detailed

**Table 2.** Results for the one-dimensional model with $1 \le R_b \le 10$, $z_\alpha = 2z_b < 1$ and seed field (17). The columns $B(0)$ and $B_r(0)$ give respectively the values of $B$ and $B_r$ at $z = 0$; $\mathcal{D} = z_\alpha^2 D$.

| $D$ | $\mathcal{D}$ | $B(0)$ | $B_r(0)$ |
|---|---|---|---|
| | $z_\alpha = 0.5,$ | $R_b = 1$ | |
| $-22$ | $-5.5$ | decays | |
| $-22.5$ | $-5.6$ | 4.9 | $-4.5$ |
| $-23$ | $-5.8$ | 5.1 | $-4.8$ |
| $-50$ | $-12.5$ | 15.5 | $-19.8$ |
| $-100$ | $-25.0$ | 34.5 | $-48.5$ |
| $-200$ | $-50.0$ | 73.8 | $-110.0$ |
| | $z_\alpha = 0.5,$ | $R_b = 3$ | |
| $-55$ | $-13.8$ | decays | |
| $-57$ | $-14.3$ | 1.0 | $-0.2$ |
| $-60$ | $-15.0$ | 1.2 | $-0.3$ |
| $-200$ | $-50.0$ | 7.2 | $-3.2$ |
| | $z_\alpha = 0.5,$ | $R_b = 5$ | |
| $-90$ | $-22.5$ | decays | |
| $-95$ | $-23.8$ | 0.6 | $-0.08$ |
| $-100$ | $-25.0$ | 0.7 | $-0.11$ |
| $-120$ | $-30.0$ | 1.1 | $-0.22$ |
| $-200$ | $-50.0$ | 2.4 | $-0.58$ |
| | $z_\alpha = 0.5,$ | $R_b = 7$ | |
| $-130$ | $-32.5$ | decays | |
| $-135$ | $-33.8$ | 0.46 | $-0.05$ |
| $-150$ | $-37.5$ | 0.63 | $-0.08$ |
| $-200$ | $-50.0$ | 1.06 | $-0.16$ |
| | $z_\alpha = 0.5,$ | $R_b = 10$ | |
| $-185$ | $-43.8$ | decays | |
| $-190$ | $-47.5$ | 0.30 | $-0.02$ |
| $-200$ | $-50.0$ | 0.37 | $-0.03$ |
| $-500$ | $-125.0$ | 1.55 | $-0.20$ |
| | $z_\alpha = 0.3,$ | $R_b = 1$ | |
| $-45$ | $-4.05$ | decays | |
| $-46$ | $-4.14$ | 3.5 | $-1.9$ |
| $-50$ | $-4.5$ | 4.8 | $-3.2$ |
| $-100$ | $-9.0$ | 17.2 | $-20.4$ |
| $-556$ | $-50.0$ | 123.0 | $-183.0$ |
| | $z_\alpha = 0.2,$ | $R_b = 1$ | |
| $-90$ | $-3.6$ | decays | |
| $-93$ | $-3.7$ | 2.9 | $-0.9$ |
| $-100$ | $-4.0$ | 4.8 | $-2.3$ |
| $-250$ | $-10.0$ | 29.5 | $-36.0$ |
| $-500$ | $-20.0$ | 66.9 | $-91.7$ |
| $-1250$ | $-50.0$ | 184.0 | $-275.0$ |
| | $z_\alpha = 0.2,$ | $R_b = 5$ | |
| $-900$ | $-36.0$ | decays | |
| $-950$ | $-38.0$ | 0.36 | $-0.014$ |
| $-1000$ | $-40.0$ | 0.48 | $-0.023$ |
| $-2000$ | $-80.0$ | 2.19 | $-0.250$ |

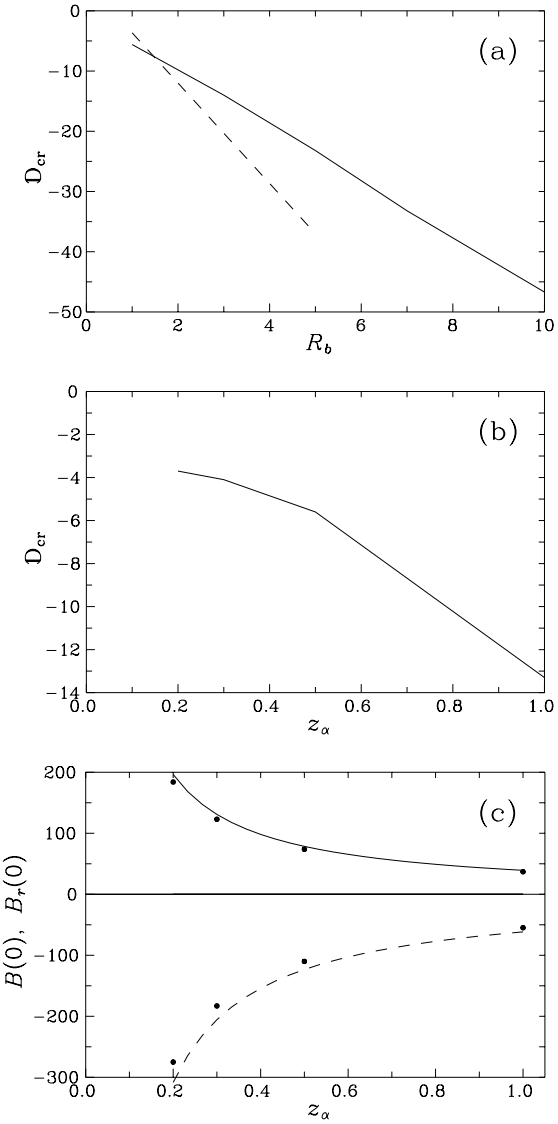


**Fig. 3a–c.** The one-dimensional model: **a** the variation of $\mathcal{D}_{\rm cr}$ with $R_b$ for $z_\alpha = 0.5$ (solid) and $z_\alpha = 0.2$ (broken), from the numerical solutions; **b** the variation of $\mathcal{D}_{\rm cr}$ with $z_\alpha$ when $R_b = 1$, from the numerical solutions; **c** $B$ (solid) and $B_r$ (broken) at $z = 0$ as functions of $z_\alpha$ for $\mathcal{D} = -50$, $R_b = 1$ from the approximate solution of Sect. 4.1 and from the numerical results (circles). In all cases $z_\alpha = 2z_b$.

dependence of $\mathcal{D}_{\rm cr}$ on $z_\alpha$ is more complicated for other values of $R_b$ (see Fig. 3a and Table 2).

### *4.4. Threshold effects*

The marginal dynamo number for the buoyant dynamo is not uniquely defined, as it depends on the strength and geometry of the seed field. Our investigations have all taken the same, arbitrary, seed field. We did note that if the value of $D$ is appreciably greater than the $D_{\rm cr}$ value of about $-13.5$ for $R_b = 1$ indicated by Table 1, even a massive increase in the seed field strength does not give rise to a nontrivial steady solution.

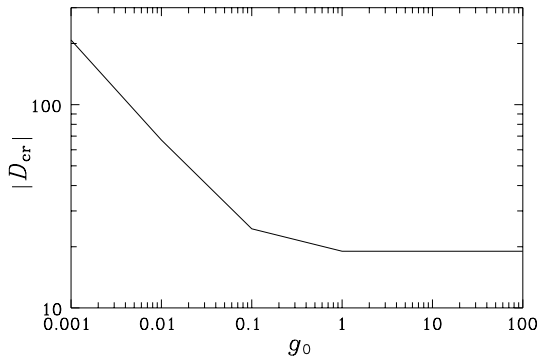


**Fig. 4.** The variation of the critical dynamo number as the strength of the seed field is altered for the one-dimensional model with $R_b = 1$ and $z_\alpha = 2z_b = 0.5$; $g_0$ controls the seed field strength – see Sect. 4.4.

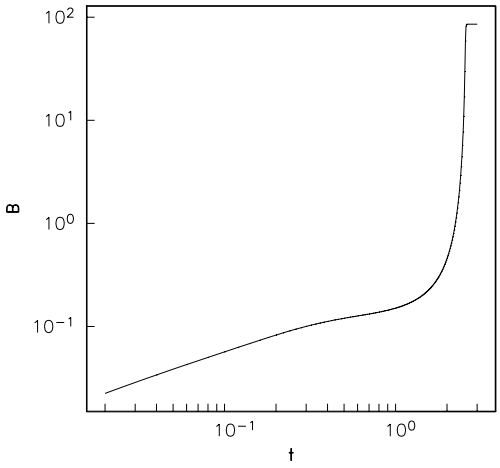


**Fig. 5.** The dependence of azimuthal field $B$ at $z = 0.02$ on time, for the one-dimensional model with $z_\alpha = 2z_b = 0.5$, $R_b = 1$, $g_0 = 10^{-3}$ and $D = -230$.

In order to investigate the threshold nature of our model more thoroughly, it is necessary to be a little more careful and systematic in the choice of the seed field. The problem is that a seed field of arbitrary spatial form contains only a relatively small projection onto the growing or steady solution. Note that we cannot cast our discussion in terms of eigensolutions in this essentially nonlinear problem. It can be expected that, if such a seed field is to have a projection large enough for excitation at small values of $|D|$, then its overall magnitude must be much greater. This results in the presence initially of large nonlinear terms in Eqs. (10) and (11), which cause numerical problems.

Thus, for the calculations discussed in this section, we chose a seed field whose form is close to that of a growing solution. We investigated the case $z_\alpha = 0.5$, $R_b = 1$, and took the seed to be approximately the steady solution at marginal excitation, multiplied by an arbitrary scale factor, $g_0$ say. The results obtained for $D_{\rm cr}$ as $g_0$ varies are shown in Fig. 4. We see that for $g_0 \lesssim 0.1$ there is a distinct threshold effect, with $D_{\rm cr} \propto g_0^{-1/2}$. For $g_0 \gtrsim 1$ the threshold effect is absent, and $D_{\rm cr}$ is almost independent of $g_0$, ie the excitation criterion is approximately independent of the seed field strength, if it is strong enough. In the first case, with a weak seed field there is an initial stage of field amplification by differential rotation, before dynamo action begins, whereas for large $g_0$, the dynamo is launched immediately. Qualitative arguments to understand this behaviour are given in Appendix B.

We show in Fig. 5 the behaviour of $B$ at a point near to $z = 0$ with time when $g_0 = 10^{-3}$. There is an initial quasi-linear growth, followed by a superexponential phase and eventual saturation. We return to this briefly in Sect. 6 and Appendix B.

### *4.5. Other calculations*

We performed calculations over the range $-1 \le z \le 1$, removing the restriction to a predetermined field parity (quadrupolar/even in the above), starting with a seed field that contained components with both odd (dipolar) and even (quadrupolar) symmetry with respect to $z = 0$. For the range of supercritical dynamo numbers investigated, the field evolved rapidly to an even parity state, corresponding to the solutions described above. This is consistent with results from calculations in $0 \le z \le 1$, with boundary conditions $\partial A/\partial z = B = 0$ on $z = 0$ appropriate to a purely odd parity field, where dynamo excitation only occurred at much larger values of $|D|$ than for the even parity solution.

We also experimented with a buoyant velocity of magnitude proportional to $B^2$. Unsurprisingly, the action of the buoyancy in limiting the field at finite amplitude was now much stronger. Our limited results strongly suggest that the overall conclusions are relatively little altered by this modification.

Another modification was to make $\alpha$ and $u_B$ proportional to the total horizontal field strength, rather than to $B$. In terms of the dimensionless quantities, we put $\alpha, u_B \propto (R_\alpha^2 B_r^2 + B^2)^{1/2}$ with $R_\alpha = 2$ and used the seed field (17). The nature of our results was little altered. For example, when $R_b = 1$, $z_\alpha = 2z_b = 0.5$, we found that the critical dynamo number changed insignificantly to $-22 < D_{\rm cr} < -21$, and that the solutions for $D = -23$ and $-50$ quite closely resembled those shown in Fig. 2.

## 5. A three-dimensional dynamo model

The mean-field dynamo equation (7) is now solved in cylindrical polar coordinates $(r, \phi, z)$ using the three dimensional mean field dynamo code described by Moss (1997). Guided by previous experience, and the results of Sect. 4.5, that quadrupolar fields are much more easily excited than dipolar, we solved Eq. (7) only in the region $z \ge 0$, using boundary conditions on $z = 0$ that impose quadrupolar parity on the solution. The code was modified to include a 'buoyant alpha' effect as in Eq. (8) and a buoyant velocity as in Eq. (9), much as described in Sect. 4, except that now we fully include the alpha-effect terms, and do not make the $\alpha\omega$ approximation. The diffusivity is assumed to depend on $z$, with

$$\eta = \eta_0 \times \begin{cases} \eta_1 , & z \le z_\eta , \\ 1 , & z \ge 2z_\eta , \end{cases} \tag{18}$$

with a smooth transition in $z_\eta < z < 2z_\eta$. The geometrical factors are taken as $f_\alpha = f_{1\alpha}(z) f_{2\alpha}(r)$ with

$$f_{1\alpha} = \begin{cases} \sin(\pi z/z_\alpha) , & z \le z_\alpha , \\ 0 , & z > z_\alpha , \end{cases}$$

$$f_{2\alpha} = \begin{cases} 1 , & r \le 0.8R , \\ (R-r)/0.2R , & r > 0.8R , \end{cases}$$

and

$$f_b = \begin{cases} z/z_b , & z \le z_b , \\ 1 , & z > z_b . \end{cases}$$

Usually, $z_\alpha = z_b = 0.12R$, $z_\eta = 0.15R$, and values $\eta_0 = 6 \times 10^{26}\,\mathrm{cm^2\,s^{-1}}$, $\eta_1 = \frac{1}{3}$ were adopted, giving a disc plane value of $\eta = 2 \times 10^{26}\,\mathrm{cm^2\,s^{-1}}$; here $R$ is the radius of the computational grid (nominal galactic radius). We used a Brandt rotation law,

$$\Omega = \frac{\Omega_0}{[1 + (r/r_\omega)^2]^{1/2}} ,$$

with $r_\omega = 0.2R$.

We scale by measuring lengths in units of $R$ and time in units of $R^2/\eta_0$. Henceforth all units are dimensionless, unless explicitly stated otherwise. The governing parameters of the problem are thus $C_\omega = \Omega_0 R^2/\eta_0$, $C_\alpha = \alpha_0 R/\eta_0$ and $C_b = q v_t R/\eta_0$. These parameters are similar to $R_\omega, R_\alpha$ and $R_b$ defined in Sect. 4, but defined in terms of a different scale length, $R$. In order to compare the three-dimensional solutions with the one-dimensional ones presented in Sect. 4, note that $R_\omega = C_\omega (h/R)^2 \eta_1^{-1}\, d(\ln\Omega)/d\ln r$, $R_\alpha = C_\alpha \eta_1^{-1} h/R$, and $R_b = C_b \eta_1^{-1} h/R$.

Eq. (7) is solved on a $N_r \times N_\phi \times N_z$ grid, covering $0 \le r \le 1$, $0 \le \phi < 2\pi$, $0 \le z \le z_m$. We adopted $C_\omega = 5 \times 10^3$, and investigated a range of values of $C_\alpha$ and $C_b$.

On $z = 0$, boundary conditions $B_z = 0$, $\partial B_r/\partial z = \partial B_\phi/\partial z = 0$ are imposed, selecting solutions with quadrupolar parity. On the other boundaries there is some freedom of choice. We use rather arbitrary open conditions on $z = z_m$, consistent with $B_r$ and $B_\phi$ going to zero at least as fast as a vacuum field. On $r = 1$, we assume that $\partial(rB_r)/\partial r = B_\phi = 0$. Previous experience with the code has shown that the solutions over the bulk of the computational volume are insensitive to the exact choice of these boundary conditions.

Preliminary calculations established that for steady solutions to be found, $z_m$ had to be 'large enough' – in practice, $z_m \gtrsim 0.4$–$0.5$. The influence of the choice of $z_m$ is discussed further in Sect. 5.1. We also verified that when $C_\alpha = 0$, solutions with decaying fields are obtained at large times, i.e. there is no spurious field amplification caused, for example, by the open boundary conditions. We found that $N_r = 31$, $N_\phi = 21$ and, with $z_m = 0.6$, $N_z = 31$ gave adequate resolution. Although the code allowed the possibility of nonaxisymmetry, we only studied axisymmetric solutions.

### 5.1. The three-dimensional solutions

We made exploratory calculations, taking $z_m = 0.6$, with several values of $C_b$ in the range 5–20. Starting from a finite amplitude seed field, containing $m = 0$ and $m = 1$ components, we found axisymmetric, steady dynamo solutions for only a limited range $C_{\alpha 1} \le C_\alpha \le C_{\alpha 2}$. For $C_\alpha < C_{\alpha 1}$, only decaying solutions were found although, as in the one-dimensional model of Sect. 4.2, the range of $C_\alpha$ values could probably have been extended to lower values with a larger seed field. For $C_\alpha > C_{\alpha 2}$, the solutions were not limited at finite amplitude, but eventually entered a phase where the fields grew without limit. When the spatial resolution was increased, $C_{\alpha 1}$ was little altered, but $C_{\alpha 2}$ did increase somewhat. Thus it is unclear whether the upper limit, $C_{\alpha 2}$, at which steady solutions are found, is a real property of our model, or due to limitations of the numerical model. (For $C_b = 10$, we found $C_{\alpha 1} \simeq 1$, $C_{\alpha 2} \simeq 5$, and the value of each of these limits increases with $C_b$.)

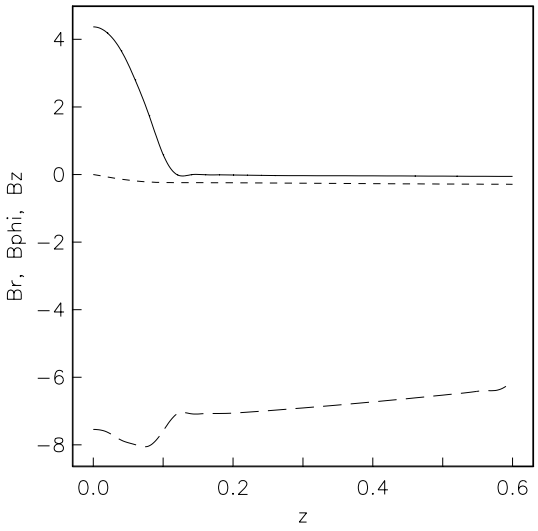


**Fig. 6.** $B_r$ (solid), $B_\phi$ (long-dashed) and $B_z$ (short-dashed) as functions of $z$ at $r \approx 0.5$ for $C_\alpha = 2$, $C_b = 10$, $C_\omega = 5 \times 10^3$, $z_\alpha = z_b = 0.12$ and $z_m = 0.6$. The signs of all the field components are the reverse of those in the one-dimensional solutions discussed above; this has no physical significance.

The unlimited field growth is undoubtedly an artefact of our simplified model, and it should not occur in more realistic models. We note that, in order to avoid a similar problem, Brandenburg et al. (1998) adopt a form for $u_B$ that grows with $B$ faster than $\alpha$. Furthermore, $\alpha$ cannot grow without bound as $B$ increases since its guaranteed upper limit is the speed of sound; this can also prevent runaway solutions.

The most noteworthy property of these models is the strong advection of azimuthal field into the halo, whilst the radial field is largely confined to the region $z \lesssim z_\alpha$. In Fig. 6 we plot $B_r$, $B_\phi$ and $B_z$ as functions of $z$ in the steady state at radius $r \approx 0.5$, for $C_b = 10$ and $C_\alpha = 2$.

The other aspects of our solutions are quite similar to those of conventional mean-field dynamo models. We present in Fig. 7 vector plots of the magnetic field in the disc plane, and in a meridian plane for a typical solution. (Note that in the latter figure, the circular plotting domain is an artefact of the graphics routine: the computations were performed in a cylindrical domain.)

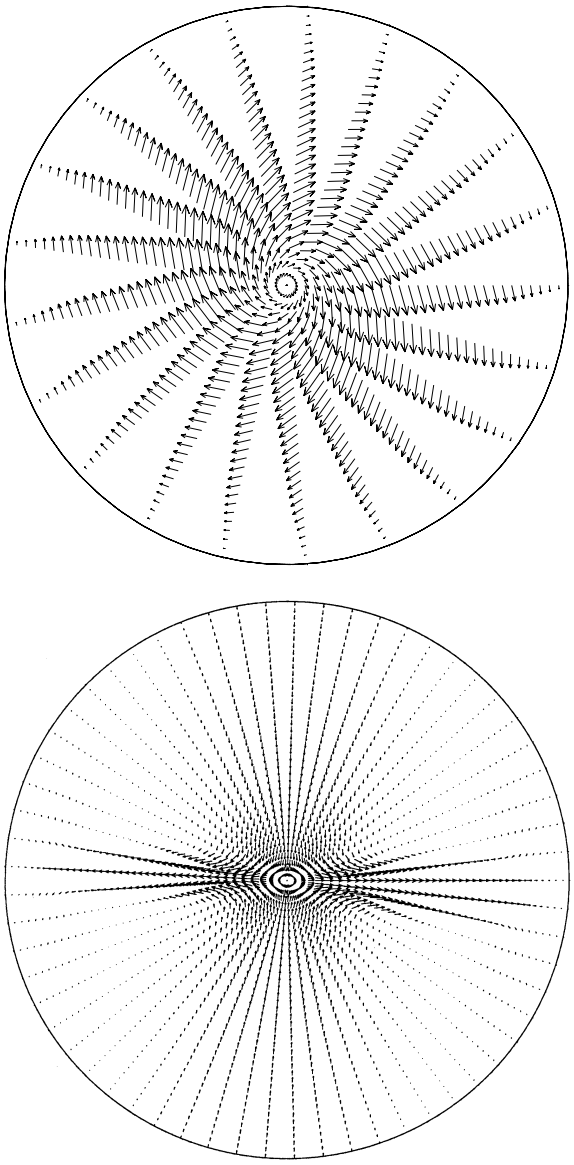

**Fig. 7.** Magnetic field vectors for $C_\alpha = 2$, $C_b = 10$, $C_\omega = 5 \times 10^3$, $z_m = 1$. *Upper panel:* the horizontal component in the disc plane; *lower panel:* the poloidal component in a meridian plane.

We also investigated the effects of moving the boundary $z = z_m$, from $z_m = 0.6$ to $z_m = 1.0$. For this test we kept the same values of $N_r$ and $N_\phi$, and the same effective spatial resolution in the $z$-direction, so we increased $N_z$ by a factor 5/3. The solutions with $z_m = 1.0$ were found to differ negligibly from those with $z_m = 0.6$ in that the fields in $z < 0.6$ were almost unaltered by this change.

## 6. Discussion

Many features of the solutions presented here resemble quite closely those of conventional galactic mean-field dynamo equations. In particular, the preferred magnetic field is of even parity, horizontal and non-oscillatory. Moreover, a negative dynamo number is required for the excitation of this field. (We have not considered here oscillatory and odd-parity solutions analytically, nor discovered numerically any oscillatory solutions.) We envisage the buoyant dynamo possibly being a continuation, in a strong field regime, of conventional mean-field dynamo action at earlier stages. Even simultaneous action of the two mechanisms may be possible. The buoyant dynamo needs a seed whose scale is comparable with that of the normal modes of the Parker instability. Therefore, in contrast to a conventional mean-field dynamo, a small-scale field cannot be a seed for the buoyant dynamo. A suitable large-scale field may be provided by a standard mean-field dynamo.

Nevertheless, some features of the buoyant dynamo discussed here are very different from those of conventional models. One such feature is not unexpected: the azimuthal field is not confined to a relatively thin disc, but pervades the halo region. This feature appears slightly more weakly in the three-dimensional model than in the one-dimensional (with $z_\alpha < 1$). However, in each case the radial field is quite strongly confined to a narrower disc region. It may be that our models overestimate the rôle of the buoyant velocity far above the disc (see the discussion at the end of Sect. 2). It can be expected that additional downward flows will also be present in this region, associated with galactic fountains. Some associated effects were discussed by Brandenburg et al. (1995).

Another difference is that in our buoyant dynamos the magnetic field has larger pitch angles $p = \arctan B_r/B_\phi$ (here $B_r$ and $B_\phi$ are dimensional) than found in the standard mean-field models. For the three-dimensional model with $C_\alpha = 2$, $C_b = 10$, $p$ typically is in the range $-(20°$–$30°)$. The one-dimensional model yields the following estimate for the pitch angle at $z = 0$ from Eqs. (15) and (16) (see also Appendix A; note that $f_\alpha/f_b \to \pi$ for $z \to 0$):

$$p = \arctan \frac{R_\alpha B_r}{B} \simeq -\arctan \frac{\pi \mathcal{R}_\alpha}{\mathcal{R}_b} \ , \tag{19}$$

where $\mathcal{R}_\alpha = R_\alpha/z_\alpha$ and $\mathcal{R}_b = R_b/z_b$ are the effective dimensionless numbers defined by analogy with $\mathcal{D}$; dimensionless field components are used in the first equality. Taking $z_\alpha = z_b$ and $R_\alpha/R_b = C_\alpha/C_b = 0.2$ as in Figs. 6 and 7, we obtain $p \simeq -30°$ in accordance with numerical results in three dimensions. Still for the nominal values $\mathcal{R}_\alpha = 3$ and $\mathcal{R}_b = 1$–$10$ estimated in Sect. 3, we obtain unrealistically large values of $p$ (for the smaller values of $R_b$) as compared with the observed values $-(10°$–$40°)$ (Beck et al. 1996). However, if a passive halo is present where $u_B \neq 0$ but $\alpha = 0$, then the pitch angle is much reduced there because the azimuthal field is still strong, but $B_r \approx 0$. When such a system is observed in synchrotron emission, the average pitch angle will be about $\langle \tan p \rangle \simeq z_\alpha \tan p$ with $z_\alpha \simeq 0.5$, in better agreement with observations.

A novel feature of our buoyant dynamos is that they can have an intermediate regime with superexponential growth, corresponding to the solution $B \propto (t - t_0)^{-1}$ of the equation $\partial B/\partial t = \alpha(B)B$ with $\alpha(B) = B$ – see Fig. 5. This may be relevant to explaining strong magnetic fields in young galaxies (Beck et al. 1996). In our models, this explosive growth is even-

tually halted by magnetic buoyancy or because $\alpha$ eventually becomes independent of the Alfvén speed.

## 7. Conclusions

We have demonstrated that an intrinsically nonlinear mean-field galactic dynamo with an alpha-effect associated with the Parker instability in the disc, and quenched by an associated buoyancy, can have steady solutions in the parameter range typical of spiral galaxies. The preferred field is non-oscillatory and has an even parity with respect to the midplane. In the one-dimensional 'local slab' models of Sect. 4, saturation seems to occur for any supercritical parameters (i.e. when the seed field strength and modulus of the dynamo number $|D|$ are large enough). In contrast, in the three-dimensional model of Sect. 5, it is unclear whether saturation can occur when $C_\alpha$ exceeds a certain value, for a given value of $C_b$.

Galactic dynamo mechanisms of this sort have been discussed by a number of authors, beginning with Parker (1992), and including Hanasz & Lesch (1998). However, to our knowledge, this is the first time that such a mechanism has been included in a complete galactic dynamo model. As mentioned in the Introduction, the concept avoids the objection raised to the standard mean field dynamo theory, that the growth of small scale field will suppress the conventional alpha-effect before the large scale field strength can approach equipartition values. The major difference in the fields calculated compared with those of earlier models, is the marked advection of field into the halo. In this, there are similarities to the calculations of Brandenburg et al. (1993), where a quasi-radial galactic wind was assumed. However, there the poloidal field was extended radially, whereas in the present case the field in the halo is almost purely azimuthal.

We realize that our models are very simple, and that we could have introduced modifications to make them arguably more realistic. However, in this investigation, we have contented ourselves with an examination of the basic properties of buoyancy driven galactic dynamos.

*Acknowledgements.* We are grateful to A. Brandenburg for helpful discussions and critical reading of the manuscript and to the referee, M. Hanasz for a number of useful comments. This work was partially supported by ECHCM contract ERBCHRXCT940483, PPARC Grant GR/L30268 and RFBR grant 96–02–16252. D.S. acknowledges financial support from the Royal Society and the University of Newcastle.

## Appendix A: an explicit form of the approximate steady state solution

For $f_\alpha$ and $f_b$ given, as in Sect. 4, by

$$f_\alpha = \begin{cases} \sin(\pi z/z_\alpha)\ , & |z| \le z_\alpha\ , \\ 0\ , & |z| > z_\alpha\ , \end{cases}$$

$$f_b = \begin{cases} z/z_b\ , & |z| \le z_b\ , \\ 1\ , & |z| > z_b\ , \end{cases}$$

where $z_b \ll z_\alpha$ are certain constants, Eq. (15) can be integrated as (with only leading terms in $z_b/z_\alpha$ retained)

$$B \approx -\pi \frac{D}{R_b^2}\frac{z_b^2}{z_\alpha} \times \begin{cases} 1\ , & z \le z_b\ , \\ 1 + \left[1 - \cos\dfrac{\pi z}{z_\alpha}\right]\dfrac{z_\alpha^2}{2\pi^2 z_b^2}\ , & z_b < z \le z_\alpha\ , \\ 1 + \dfrac{z_\alpha^2}{\pi^2 z_b^2}\ , & z_\alpha < z \le 1\ , \end{cases}$$

$$B_r \approx \pi^2 \frac{D}{R_b^3}\frac{z_b^3}{z_\alpha^2} \times \begin{cases} 1\ , & z \le z_b\ , \\ \dfrac{z_\alpha}{\pi}\left[1 + \dfrac{z_\alpha^2\,(1-\cos\pi z/z_\alpha)}{2\pi^2 z_b^2}\right]\sin\dfrac{\pi z}{z_\alpha}\ , & z_b < z \le z_\alpha\ , \\ 0\ , & z_\alpha < z \le 1\ . \end{cases}$$

## Appendix B: the marginal dynamo number

The approximate steady-state solution developed in Sect. 4.1 cannot be used to estimate the marginal dynamo number. Here we obtain a very crude approximation which demonstrates the connection between the critical dynamo number and the initial magnetic field. Let us replace $\partial/\partial z$ by $1/L$ and $\partial^2/\partial z^2$ by $-1/L^2$ in Eqs. (10) and (11), where $L$ is some characteristic scale. With such a simplistic approach, we replace $f_b$ and $f_\alpha$ by unity. Consider the marginal case $\partial \boldsymbol{B}/\partial t = 0$ with $B > 0$ (we recall that $B$ denotes the azimuthal field component). We deal with the result as with a system of linear equations for $A$ and $B$, albeit with its coefficients as functions of $B$. This yields the following 'dispersion relation':

$$D_{\rm cr} B + L^{-1}(R_b B + L^{-1})^2 = 0\ . \tag{B1}$$

First assume that the initial magnetic field is weak, $B \ll (R_b L)^{-1}$. Then

$$D_{\rm cr} \propto B^{-1}\ .$$

Here the marginal strength of the magnetic field at which the buoyant dynamo is launched differs from the seed field because the latter can be amplified by differential rotation prior to the start of the dynamo action. This intermediate regime with $B$ growing linearly in time can be seen in one-dimensional simulations discussed in Sect. 4, see also Fig. 5. Thus, we have $B \simeq R_\omega B_0 t$, where $B_0$ is the seed field. Replacing $R_\omega$ by $D_{\rm cr}/R_{\alpha\,{\rm cr}}$, we have

$$D_{\rm cr} \propto B_0^{-1/2}$$

as obtained in the numerical solutions of Sect. 4.4, with $B_0$ replaced by $g_0$, for a weak seed field (note that $D_{\rm cr} < 0$).

The other solution of Eq. (B1), $B = O(DR_b^{-2})$, obtained for $R_b B \gg 1$, is the steady-state solution (15). If the seed field is stronger than this, it decays until it reaches this steady state.

Consider now a seed field of intermediate strength, $B = O(DR_b^{-2})$; then the dynamo can operate in an optimal regime where the field growth time $\tau_B$ is minimum. The growth time can be estimated from a similar 'dispersion relation' for Eqs. (10)

and (11) by replacing $\partial/\partial t$ by $1/\tau_B$, $\partial/\partial z$ by $1/L$ and $\partial^2/\partial z^2$ by $-1/L^2$ as

$$\tau_B^{-1} \simeq (-DBL^{-1})^{1/2} - R_b B L^{-1} - L^{-2} \ ,$$

so that the minimum value of $\tau_B$ is $\tau_{\rm min}^{-1} \simeq -\frac{1}{4} D R_b^{-1} - L^{-2}$. The marginal effective dynamo number then follows from $\tau_{\rm min}^{-1} = 0$ as

$$\mathcal{D}_{\rm cr} \simeq -4 R_b \ , \qquad \text{(B2)}$$

where we have taken $L = z_\alpha$. This agrees (rather remarkably well!) with the results of Sect. 4.4 (see Figs. 3a,b), at least if $R_b = 1$ (the only case that we investigated in sufficient detail).

## References


Beck R., Brandenburg A., Moss D., Shukurov A., Sokoloff D.D., 1996, ARA&A 34, 155

Brandenburg A., 1994, In: Proctor M.R.E., Gilbert A.D. (eds.) Lectures on Solar and Planetary Dynamos. Cambridge University Press, Cambridge, p. 17

Brandenburg A., Donner K-J., Moss D., et al., 1993, A&A 271, 36

Brandenburg A., Moss D., Shukurov A., 1995, MNRAS 276, 651

Brandenburg A., Saar S.H., Turpin C.R., 1998, ApJ 498, L51

Childress S., Gilbert A., 1995, Stretch, Twist, Fold: The Fast Dynamo. Springer, Berlin

Elstner D., Rüdiger G., Schultz M., 1996, A&A 240, 289

Ferriz-Mas A., Schmitt D., Schüssler M., 1994, A&A 289, 949

Hanasz M., Lesch H., 1993, A&A 278, 561

Hanasz M., Lesch H., 1998, A&A 332, 77

Hurewicz W., 1958, Lectures on Ordinary Differential Equations. MIT, Cambridge Mass.

Jennings R., Weiss N., 1991, MNRAS, 252, 249

Ko C.M., Parker E.N., 1989, ApJ 341, 828

Krause F., Rädler K.-H., 1980, Mean-Field Magnetohydrodynamics and Dynamo Theory. Pergamon Press, Oxford

Kvasz L., Sokoloff D., Shukurov A., 1992, Geophys. Astrophys. Fluid Dyn. 65, 231

Moffatt H.K., 1978, Magnetic Field Generation in Conducting Fluids. Cambridge University Press, Cambridge

Moss D., 1997, MNRAS, 289, 554

Moss D., Tuominen I., Brandenburg A., 1990a, A&A 228, 284

Moss D., Tuominen I., Brandenburg A., 1990b, A&A 240, 142

Moss D., Shukurov A., Sokoloff D.D., Berkhuijsen E.M., Beck R., 1998, A&A 335, 500

Nozakura T., 1991, MNRAS 248, 389

Nozakura T., 1993, MNRAS 262, 970

Parker E.N., 1979, Cosmical Magnetic Fields. Clarendon Press, Oxford

Parker E.N., 1992, ApJ 401, 137

Rädler K.-H., 1968, Z. Naturforsch. 23, 1851

Rädler K.-H., 1990, In: Berthomieu G., Cribier M. (eds.) Inside the Sun. IAU Colloq. 121, Kluwer, Dordrecht, p. 385

Roberts P.H., Soward A.M., 1975, Astron. Nachr. 296, 49

Ruzmaikin A.A., Shukurov A.M., Sokoloff D.D., 1988, Magnetic Fields of Galaxies. Kluwer, Dordrecht

Schmitt D., 1987, A&A 174, 281

Schmitt D., Schüssler M., 1989, A&A 223, 343

Schüssler M., 1993, In: Krause F., Rädler K.-H., Rüdiger G.R. (eds.) The Cosmic Dynamo. IAU Symp. 157, Kluwer, Dordrecht, p. 27

Thelen J.-C., 1997, Acta Astron. Geophys. Univ. Comenianae 19, 221

Vainshtein S.I., Cattaneo F., 1992, ApJ 393, 165

Vainshtein S.I., Zeldovich Ya.B., 1972, Sov. Phys. Usp. 15, 159

Zeldovich Ya.B., Ruzmaikin A.A., Sokoloff D.D., 1983, Magnetic Fields in Astrophysics. Gordon and Breach, New York